Comparative electrochemical oxidation of methyl orange azo dye using Ti/Ir-Pb, Ti/Ir-Sn, Ti/Ru-Pb, Ti/Pt-Pd and Ti/RuO_2 anodes

Eloy Isarain-Chavez[a, □], Maria Dolors Baro[a], Emma Rossinyol[b], Ulises Morales-Ortiz[c], Jordi Sort[a, d], Enric Brillas[e, □, 1], Eva Pellicer[a, □]

[a] *Departament de Física, Universitat Autònoma de Barcelona, E–08193 Bellaterra, Spain*
[b] *Servei de Microscòpia, Universitat Autònoma de Barcelona, E–08193 Bellaterra, Spain*
[c] *Departamento de Química, Universidad Autónoma Metropolitana–Iztapalapa. Av. San Rafael Atlixco No. 186, CP. 09340, Mexico DF, Mexico*
[d] *Institució Catalana de Recerca i Estudis Avançats (ICREA), Pg. Lluís Companys 23, E-08010 Barcelona, Spain*
[e] *Laboratori d'Electroquímica dels Materials i del Medi Ambient, Departament de Química Física, Facultat de Química, Universitat de Barcelona, Martí i Franquès 1–11, 08028 Barcelona, Spain*

A B S T R A C T

The relative oxidation power of dimensionally stable anodes, namely Ti/Ir-Pb, Ti/Ir-Sn, Ti/Ru-Pb, Ti/Pt-Pd and Ti/RuO_2, has been determined from the anodic oxidation (AO) treatment of 2 dm^3 of methyl orange azo dye solutions in 0.050 mol dm^{-3} Na_2SO_4 of pH 7.0 at constant current density. The anodes were synthesized by the dip-coating method using the corresponding metallic chlorides in isopropanol/water and their morphology, surface roughness, crystallographic structure and composition were analyzed. A mixture of IrO_2, Pb_2O_3 and Pb_3O_4 were the components in the outperforming Ti/Ir-Pb anode. The effect of current density, Na_2SO_4 concentration, and cathode nature on the decolorization of azo dye solutions by AO with Ti/RuO_2 was examined. Under favorable conditions, 96%-98% color removal was achieved using Ti/Ir-Pb, Ti/Ir-Sn and Ti/Ru-Pb, with lower decolorization for Ti/Pt-Pd and Ti/RuO_2 anodes. In all cases, a pseudo-first-order decolorization process was found. The oxidation ability of anodes rose in the order Ti/RuO_2 < Ti/Pt-Pd < Ti/Ru-Pb < Ti/Ir-Sn < Ti/Ir-Pb, achieving 76.0% mineralization for the latter electrode. The mixture of active and non-active materials then gave rise to anodes with higher oxidation power than those made solely of active materials, due to the enhancement of the oxidation action of hydroxyl radicals formed in the non-active oxide. The superiority of Ir over Ru in the mixed metal oxides was related to the greater adsorption of organics on its surface, thereby favoring their oxidation. Ammonium and sulfate ions were released as pre-eminent ion. Stable byproducts and final short-linear aliphatic carboxylic acids were identified by gas chromatography-mass spectrometry and ion-exclusion high-performance liquid chromatography. Based on these compounds, a reaction sequence for methyl orange mineralization is proposed.

Introduction

There is an increasing interest in the study of the destruction of organic pollutants from wastewaters by means of anodic oxidation (AO). This environmentally friendly method is an electrochemical advanced oxidation process (EAOP) based on the in situ generation of hydroxyl radical (•OH) at the anode surface [1-7]. This radical has a high standard reduction potential (E° (•OH/H_2O) = 2.80 V/SHE) with a very short half-life of 10^{-4} s and can react with organics in a non-selective manner until full conversion into CO_2 and inorganic ions take place. These reactions originate organic intermediates, which tend to be less harmful to the aquatic environment. AO can be applied to wastewaters with high chemical oxygen demand (COD) and total organic carbon (TOC), low biodegradability and toxic pollutants, working at intermediate temperatures [5,7,8]. For a high O_2-overvoltage metal oxide (MO) anode, the initial water oxidation yields the physisorbed MO_x(OH) by reaction (1), which can be subsequently oxidized to the chemically adsorbed "superoxide" MO_{x+1} by reaction (2) [5-9]:

$$MO_x + H_2O \rightarrow MO_x(OH) + H^+ + e^- \quad (1)$$
$$MO_x(OH) \rightarrow MO_{x+1} + H^+ + e^- \quad (2)$$

Depending on the predominance of either reaction (2) or reaction (1) at the anode surface, the anodes are classified as active or non-active [8,10], respectively. In active MO anodes like Pt, IrO_2, and RuO_2, MO_{x+1} is formed at a much larger extent than $MO_x(OH)$ and it oxidizes the aromatic organics to final carboxylic acids with relatively low mineralization. In contrast, $MO_x(OH)$ is pre-eminently formed in non-active MO anodes like SnO_2 and PbO_2, and this physisorbed radical reacts more effectively with most aromatics and aliphatic compounds leading to their total mineralization or incineration. The best non-active anode is currently considered the boron-doped diamond (BDD) thin-films electrode, where only reaction (1) occurs, presenting a higher O_2-overvoltage than Pt and conventional MO anodes [5,11-14].

Azo dyes are the most used dyes worldwide [15]. They are composed of a complex chemical structure with one or various azo groups (N N-) as chromophore, which are linked to aromatic systems with lateral groups including OH and $-SO_3^-$, among others [5,16]. Azo dyes are extensively used in textile industries, which discharge large volumes of highly colored effluents with dye contents up to 250 mg dm^{-3} and other toxic components [17,18]. These wastewaters cause aesthetic problems and scarce light penetration in water bodies, along with health problems to aquatic living beings due to their carcinogenic, toxic and mutagenic properties [19,20]. Azo dyes persist largely in the aquatic environment due to their resistance to biodegradation and poor removal by physicochemical and biological treatments in wastewater treatment plants [21,22]. Powerful oxidation methods are then needed to destroy these pollutants from wastewaters to avoid their dangerous effects on living beings.

The effectiveness of AO with dimensionally stable anodes to decolorize and partially mineralize dye solutions in the presence of sulfate or chloride ions has been well proven [5]. Active MO such as Ti/RuO_2 [3], Ti/IrO_2 [23,24] and Ti/Pt [25], non-active MO like Ti/PbO_2 [9,26] and active mixed MO (MMO) such as Ti/Ru-Ti [25,27], Ti/Ir-Ru [28], Ti/Sn-Sb-Pt [29] and C/Pt-Bi [30] have been utilized. Faster decolorization was found in chloride compared to sulfate medium due to the Cl^- oxidation to active chlorine (Cl_2/HClO/ClO^-), which attacks the organics much more rapidly than $MO_x(OH)$ formed from reaction (1) [5,7,8]. Greater production of active chlorine occurs in active anodes, but the main drawback of using such oxidants is the formation of toxic and persistent chloroderivatives that are slowly removed. For a Ti/IrO_2 anode, for example, Zaviska et al. [23] found 99% color removal with 51% COD and 75% TOC decays for a 25 mg dm^{-3} methyl violet 2 B solution in 3.42 mmol dm^{-3} NaCl operating at a current density (j) of 15 mA cm^{-2} for 40 min, whereas Wang et al. [24] reported 99% color removal with 84% COD abatement for a 100 mg dm^{-3} methylene blue solution in 1 g dm^{-3} NaCl of pH 7 at j = 42.8 mA m^{-2} after only 20 min of electrolysis. The use of non-active anodes in chloride-free medium, where only reactions (1) and/or (2) generate the oxidants, can yield larger mineralization but require much longer electrolysis time. Panizza and Cerisola [9] described the achievement of 90% COD removal for 200 mg dm^{-3} methyl red, at similar rate within a pH range of 3 to 7 regulated with H_2SO_4 or NaOH, using BDD and Ti/PbO_2 anodes at applied current of 0.5 A for 8 h. Similarly, Carvalho et al. [26] obtained total decolorization and 70% TOC decay when treating a 300 mg dm^{-3} methyl green solution in 0.50 mmol dm^{-3} H_2SO_4 with Ti/PbO_2 at j = 40 mA cm^{-2} for 400 min.

Little is known about the comparative degradation of dye solutions by AO using different MMO anodes, where the nature of the

mixed oxides may play an important role in the degradation process in chloride-free solution. To gain a better understanding on the behavior of MMO electrodes, we have prepared five dimensionally stable anodes onto Ti substrate including mixtures of active IrO_2 and RuO_2 with non-active PbO_2 and SnO_2 (Ti/Ir-Pb, Ti/Ir-Sn and Ti/Ru-Pb) and Pt with Pd (Ti/Pt-Pd) to be compared with a typical active Ti/RuO_2. The oxidation power of these anodes was assessed tak ing methyl orange azo dye as a model molecule. Methyl orange (sodium 4-{[4-(dimethylamino)phenyl]diazenyl}benzene-1-sulfonate, $Na^+C_{14}H_{14}N_3O_3S^-$, Color Index number = 13025, M = 327.3 g mol^{-1}) presents a red quinone-type structure in acidic medium and a yellow azo-type one under alkaline conditions. It is not biodegradable and possesses mutagenic properties [31]. The degradation of this compound has been reported by different methods such as activated carbon with Fe_3O_4 [32], ozonation combined with ultrasonic irradiation [33], photocatalysis with TiO_2 [34-36], sonophotocatalysis [37], UV/H_2O_2 [38], wet oxidation [39] and Fenton's reagent [40]. Several studies have examined the AO treatment of methyl orange solutions with BDD [3,41], Ti/RuO_2 [3], C/Pt-Bi [30], Ti filter electrodes arrays [42] and exfoliated graphite [43].

This paper presents a study on the comparative oxidation of methyl orange in sulfate solution of pH 7.0 by AO with Ti/Ir-Pb, Ti/Ir-Sn, Ti/Ru-Pb, Ti/Pt-Pd and Ti/RuO_2. These dimensionally stable anodes were synthesized and their morphology, surface roughness, crystallographic structure and composition were analyzed. The effect of j, Na_2SO_4 concentration and cathode used on color removal and mineralization rate was examined. Stable byproducts were identified by gas chromatography-mass spectrometry (GC-MS) and the evolution of final carboxylic acids was followed by high-performance liquid chromatography (HPLC). A reaction sequence for methyl orange mineralization is finally proposed based on all the byproducts detected.

2. Experimental

2.1. Chemicals

Methyl orange of 99% purity was supplied by the pharmaceutical Karal (Mexico). Sulfuric acid and anhydrous sodium sulfate were of analytical grade and purchased from KEM and Fluka, respectively. Carboxylic acids were of analytical grade supplied by Aldrich. All solutions were prepared with pure water obtained from an EDM Millipore Elix-5 system with resistivity > 18MΩ cm at 25 °C and < 30 ppb of TOC. Organic solvents and other chemicals used in HPLC and GS-MS were purchased from Merck, Fluka and Aldrich.

2.2. Anodes synthesis

The dimensionally stable anodes were prepared using ASTM grade 2 titanium plates as substrates of 6 cm × 28 cm × 0.1 cm in dimension. The RuO_2 film was synthesized at room temperature by dipping the substrate in isopropanol/water mixture with 0.1 mol dm^{-3} $RuCl_3 \cdot xH_2O$ to form from 8 to 10 consecutive layers. Each coating was dried at 100 °C during 10 min before the next deposition and the resulting film was annealed for 1 h at 500 °C in air to form the RuO_2 phase [44]. The electrodes of Ti/Ir-Pb, Ti/Ir-Sn, Ti/Ru-Pb and Ti/Pt-Pd were prepared following an analogous synthetic method with $IrCl_3 xH_2O$, $PbCl_2$, $SnCl_2$, $Na_2PtCl_6 xH_2O$, Na_2PdCl_4 and $PdCl_2$ in isopropanol/water mixture.

2.3. Anodes characterization

The chemical composition of all the dimensionally stable anodes was determined by energy dispersive X-ray spectroscopy (EDX). The Ir-Pb based coating formed on the Ti substrate (i.e., the outperforming anode) was subjected to an in-depth morphological and structural characterization. Its morphology was characterized by field emission scanning electron microscopy (FE-SEM) using a Merlin Zeiss microscope operated at 5 kV and surface roughness was measured on a confocal 3D optical surface metrology system LEICA DCM3D. The crystallographic structure of the coating was determined by X-ray diffraction (XRD) on a Philips X'Pert Diffractometer in Bragg-Brentano geometry using Cu Kα radiation (1.542 A) in the 2θ range from 10° to 90° with 0.03° as step size and 10 s holding time. And by high-resolution transmission electron microscopy (HRTEM) using a Jeol-JEM-2011 microscope at 200 kV. For TEM observation, the Ti/Ir-Pb sample was subjected to ultrasonication for 20 min in isopropyl alcohol to favor the detachment of the coating and then two drops of the suspension were placed onto a holey carbon-coated Cu TEM grid.

2.4. Electrolytic system

Electrolysis tests were carried out in an undivided thermostated tank reactor containing 2 dm^3 of methyl orange solution in neutral aqueous media with 0.050 or 0.50 mol dm^{-3} Na_2SO_4. The solution was vigorously stirred with a magnetic stirrer at 500 rpm at a temperature of 25 °C. Synthesized Ti/Ir-Pb, Ti/Ir-Sn, Ti/Ru-Pb, Ti/Pt-Pd or Ti/RuO_2 electrode was used as anode, whereas a Ti/RuO_2, Ti or 316 stainless steel electrode was employed as cathode. The geometric area of all electrodes in contact with the solution was 140 cm^2 and the interelectrode gap was about 1.0 cm. Trials were run at constant j provided by a BK Precision Model 1900 (DC 1-16 V, 60 A) power supply, which displayed directly the potential difference between electrodes.

2.5. Analytical methods

The conductivity, pH and temperature of the initial and treated solutions were measured with a HACH Sension 156 portable multiparameter. The loss in color of methyl orange solutions was monitored from the drop in absorbance at its maximum wavelength (λ_{max}) of 465 nm measured with a Thermo Scientific Evolution 300 UV/Vis spectrophotometer thermostated at 25 °C. The decolorization efficiency or percentage of color removal was calculated from the initial absorbance (A_0) and its value at time t (A) as follows [5,45]:

$$\text{Percentage of color removal} = \frac{A_0 - A}{A_0} \times 100 \quad (3)$$

The mineralization of dye solutions was followed from the abatement of their TOC measured on a Shimadzu L-CSN TOC analyzer. Before this analysis, the samples were filtered with 0.45 μm PTFE filters from Whatman and 50 μL aliquots were injected into the TOC analyzer, always obtaining an accuracy of ⍰1%. Total nitrogen (TN) was obtained with a Shimadzu TNM-1 unit coupled to the above analyzer. Assuming that the theoretical total mineralization of methyl orange involves its transformation into carbon dioxide and ammonium and sulfate ions, as will be discussed below:

$C_{14}H_{14}N_3O_3S^- + 29\ H_2O \rightarrow 14\ CO_2 + 3\ NH_4^+ + SO_4^{2-} + 60\ H^+ + 62\ e^-$ (4)

the mineralization current efficiency (MCE) at applied current I (in A) and electrolysis time t (in h) was estimated from Eq. (5) [45,46]:

$$\%\,\mathrm{MCE} = \frac{nFV_s\Delta(\mathrm{TOC})_{\mathrm{exp}}}{4.32\times10^7 mIt}\times 100 \quad (5)$$

where $n = 62$ is the number of electrons of the complete mineralization process, F is the Faraday constant (96,487C mol^{-1}), V_s is the solution volume (in dm^3), $\Delta(TOC)_{exp}$ is the experimental TOC decay (in mg dm^{-3}), 4.32×10^7 is a conversion factor (3600 s h^{-1} × 12000 mg C mol^{-1}) and $m = 14$ is the number of carbon atoms of the azo dye.

Generated carboxylic acids were identified and quantified by ion-exclusion HPLC using a Waters 600 LC coupled with a Waters 996 photodiode array detector set at λ = 210 nm. Aliquots of 20 μL were injected into the LC fitted with a Bio-Rad Aminex HPX 87H, 300 mm × 7.8 mm, column at 35 °C and a 4 mmol dm^{-3} H_2SO_4 solution at 0.6 cm^3 min^{-1} circulated as mobile phase. Chromatograms exhibited well-defined peaks related to oxalic (retention time, t_r = 6.5 min), oxamic (t_r = 9.1 min), malic (t_r = 9.7 min), succinic (t_r = 12.2 min) and acetic (t_r = 14.8 min) acids.

The NO_2^-, NO_3^- and SO_4^{2-} concentrations were obtained by ion chromatography upon injection of 25 μL samples into a Shimadzu 10Avp LC coupled to a Shimadzu CDD 10Avp conductivity detector. The LC was fitted with a Shim-Pack IC-A1S, 100 mm × 4.6 mm, anionic column at 40 °C and a mobile phase with boric acid, sodium gluconate, sodium tetraborate, acetonitrile, butanol and glycerine was eluted at 2.0 cm^3 min^{-1}. The NH_4^+ content was determined spectrophotometrically from the standard indophenol blue reaction.

To identify stable intermediates, a 50 mg dm^{-3} dye solution was treated by AO using the Ti/Ir-Pb anode at j = 70 mA cm^{-2} and samples of 100 cm^3 were withdrawn at several electrolysis times. Their organic components were extracted with 3 × 10 cm^3 of CH_2Cl_2, dried over anhydrous Na_2SO_4, filtered and concentrated to about 1 cm^3 to be analyzed by GC-MS. This was made with an Agilent Technologies system composed of a 7890 B GC, fitted with a non-polar Agilent J&W HP-5 ms Teknokroma Sapiens-X5 ms 0.25 μm, 30 m × 0.25 mm, column, and a 5975C MS operating in EI mode at 70 eV. The temperature ramp was 50 °C for 2 min, 15 °C min^{-1} up to 290 °C and hold time 5 min. The mass spectra were identified using a NIST05-MS library.

3. Results and discussion

3.1. Morphological and compositional characterization of synthesized Ti/Ir-Pb film

Fig. 1a shows a representative FE-SEM image of the synthesized Ir-Pb coating onto Ti substrate. The film looks homogeneous, nevertheless a close-up view of the coating (inset panel of Fig. 1a) indicates the presence of irregular granules, resembling the cobblestone morphology, along with defects like holes and tiny cracks. This peculiar morphology can be understood considering that: (i) the coating is not fully crystallized (which is not the case as it will be shown later) or either (ii) imperfections in the contact area (heat stress) are generated during the thermal decomposition of the oxide precursors onto the Ti substrate. Surface roughness was quantified by confocal microscopy [47].

Fig. 1b shows the topographical image of a selected coating's area of 157.5 μm2, characterized by Sa = 0.14 μm (arithmetic mean of the surface roughness), Sq = 0.18 μm (standard deviation of the distribution curve), Sp = 1.18 μm (maximum peak height) and Sz = 1.84 μm (amplitude between the highest peak and the deepest valley) (see Table S1 in Supplementary Material). Fig. 1c depicts microscopy [47]. Fig. 1b shows the topographical image of a selected coating's area of 157.5 μm2, characterized by Sa = 0.14 μm (arithmetic mean of the surface roughness), Sq = 0.18 μm (standard deviation of the distribution curve), Sp = 1.18 μm (maximum peak height) and Sz = 1.84 μm (amplitude between the highest peak and the deepest valley) (see Table S1 in Supplementary Material). Fig. 1c depicts

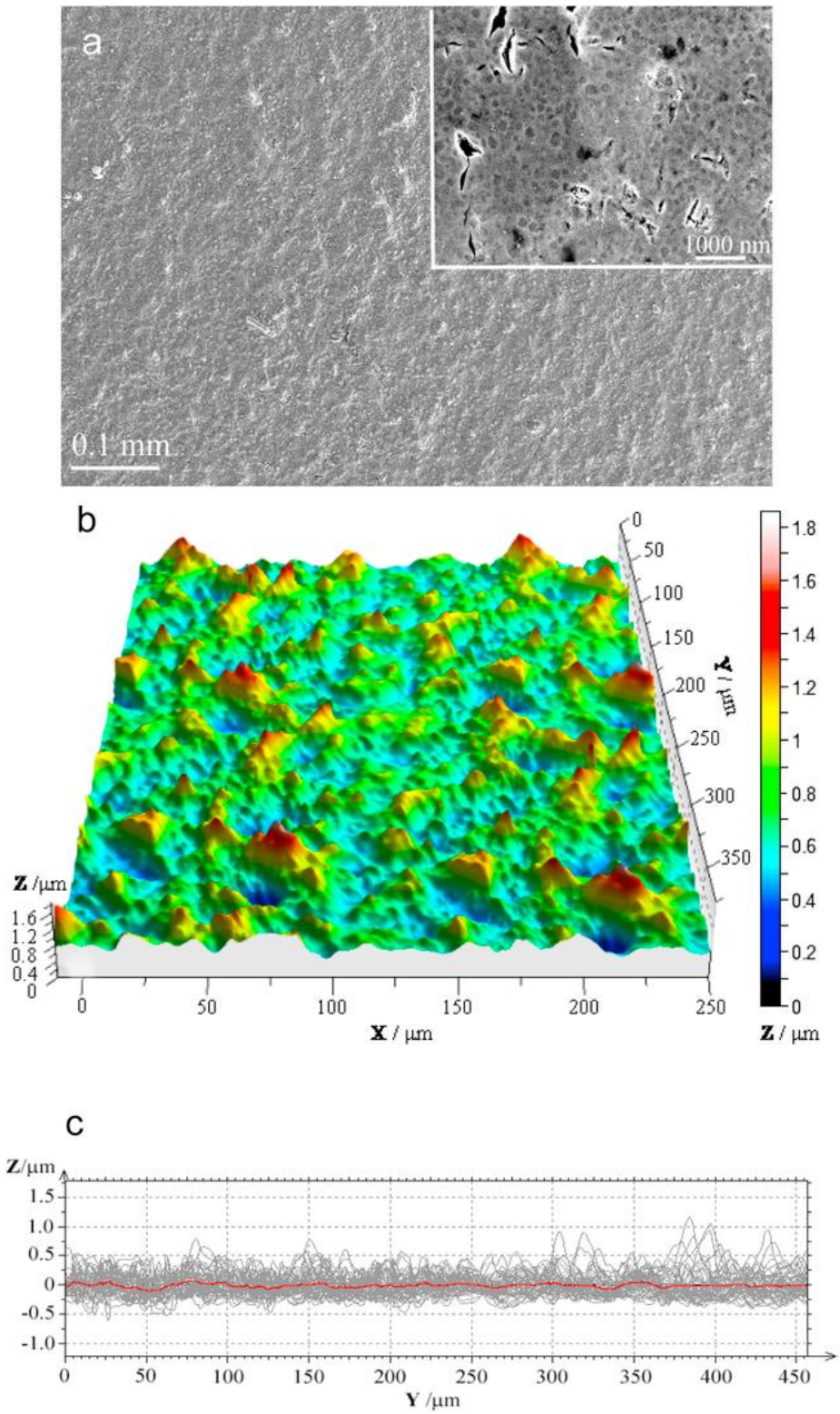

Fig. 1. (a) FE-SEM image showing the morphology for the synthesized Ti/Ir-Pb anode (the inset panel presents a detailed view). Confocal images showing: (b) profiling topographical image in 3D for an area of 157.5 μm^2 and (c) aleatory profile of cut hollow.

an aleatory profile taken across the films' surface. The related parameters are listed in Table S1 and are in agreement with those mentioned above. Fig. S1a of Supplementary Material shows the Abbott-Firestone curve with an increase in granule sizes from 0.275 to 2.753 μm and a material ratio calculated of 1.37 μm above the lowest peak corresponding to 18% and 1.92 μm below the highest peak related to 78%. The peak count histogram of Fig. S1b highlights the

existence of grains from 0.00175 to 0.003 μm^{-2} for peaks from 0.9 to 1.5 μm. Hence this film morphology, results rather large surface area, which could favor the occurrence of catalytic sites for O_2 evolution and, thereby, the generation of M(OH) radicals at the surface. In order to determine the chemical composition of the Ti/Ir-Pb film, an EDX analysis was conducted. The EDX pattern (Fig. 2a) confirmed the existence of Ti, Ir and Pb along with O, thereby suggesting the formation of PbO_x, and IrO_x species onto the Ti substrate. The occurrence of metal oxides makes sense considering that the thermal decomposition of precursors was performed in air. Table 1 lists the weight and atomic percent of all elements present in the synthesized MO and MMO coatings, including the Ti/Ir-Pb electrode, as determined by EDX.

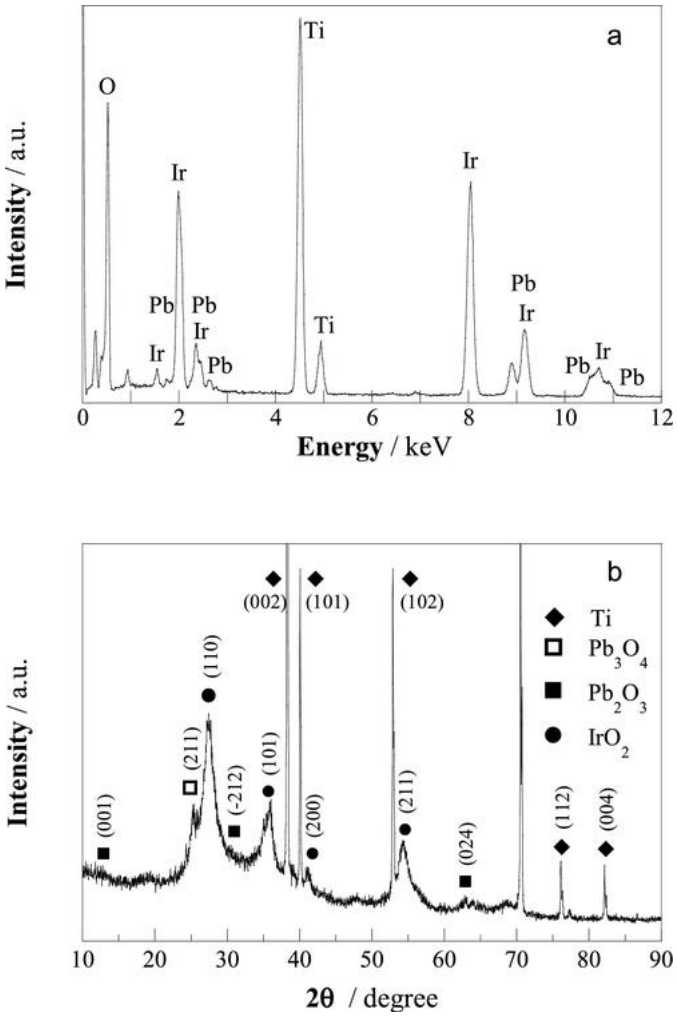

Fig. 2. (a) EDX patterns showing the peaks characteristic for Ir, Pb and O for the Ti/Ir-Pb film. (b) XRD patterns of Ti/Ir-Pb film related to the crystallographic planes of IrO_2, Pb_2O_3, Pb_3O_4 and Ti.

Table 1
Weight and atomic percent of the elements contained in the synthesized MO and MMO films onto Ti substrate determined by energy-dispersive X-ray analysis.

	Ti/Ir-Pb		Ti/Ir-Sn		Ti/Ru-Pb		Ti/RuO_2		Ti/Pt-Pd	
Element	wt%	at.%	wt%	at.%	wt%	at.%	wt%	at.%	wt%	at.%
O	28.8	65.7	32.7	71.2	24.7	65.7	25.1	56.9	54.9	85.6
Ti	36.6	27.9	27.1	19.7	5.6	5.0	38.1	29.3	21.0	11.1
Ir	25.1	4.7	23.7	4.3	-	-	-	-	-	-
Pb	9.5	1.7	-	-	0.6	0.2	-	-	-	-

Sn	-	-	16.5	4.8	-	-	-	-	-	-
Ru	-	-	-	-	69.1	29.1	36.9	13.7	-	-
Pd	-	-	-	-	-	-	-	-	2.1	0.5
Pt	-	-	-	-	-	-	-	-	22.0	2.8

The XRD pattern of the Ir-Pb film is shown in Fig. 2b. The pattern displays several peaks with dissimilar width. The narrow reflections are assigned to the metallic Ti substrate underneath the coating. Two different Pb oxides, which were identified as Pb_2O_3 and Pb_3O_4, are present in the diffractogram. Peaks at 2θ values of 12.7°, 29.5° and 62.8° correspond to the (001), (-212) and (024) planes, respectively, of monoclinic Pb_2O_3 phase. Meanwhile, the peak at 2θ = 26.3° matches the (211) plane of tetragonal Pb_3O_4. Regarding iridium oxides species, peaks placed at 2θ values of 28.0°, 34.7°, 40.1° and 54.1° are assigned to the (110), (101), (200) and (211) planes, respectively, of IrO_2.
The structure of the Ir-Pb oxide film was further verified by TEM. Upon sonication, a few coating fragments became detached from the Ti substrate (Fig. 3a). A detailed analysis of these fragments revealed the presence of crystalline particles with a diameter from 2 nm to 15 nm, in agreement with the peaks observed by XRD. From the lattice fringes depicted in Fig. 3b and 3c, the presence of lead and iridium oxides was confirmed. In particular, the interplanar distances indicated in Fig. 3b correspond to (-212) of Pb_2O_3 (JCPDS 23-0331) and (211) of Pb_3O_4 (JCPDS 41-1493). Likewise, two interplanar distances assigned to the (200) and (110) planes of the IrO_2 (JCPDS 15-0870) are shown in the HRTEM image of Fig. 3c. Finally, the selected area electron diffraction (SAED) pattern of Fig. 3d, taken on an aggregate of particles, showed spotty rings. The different spots were well assigned to the Pb_2O_3, Pb_3O_4 and IrO_2 components.

3.2. Decolorization of methyl orange solutions with Ti/RuO_2 anode

Firstly, the effect of important operation variables over the decolorization of methyl orange solutions by means of AO was investigated using the synthesized active Ti/RuO_2 anode. The assays were made at pH 7.0 and 25 °C for 240 min, with continuous pH regulation by addition of small volumes of 0.1 mol dm^{-3} NaOH.
The current density is a key parameter in AO because it regulates the amount of oxidizing species produced at the anode surface from reactions (1) and (2). The influence of this variable was tested for 2 dm^3 of a 30 mg dm^{-3} methyl orange solution in 0.050 mol dm^{-3} Na_2SO_4 with a Ti/RuO_2 anode and a 316 stainless steel cathode at j values between 7.1 and 70 mA cm^{-2}. Fig. 4a depicts the percentage of color removal in front of electrolysis time for these experiments. As can be seen, the color at λ_{max} = 465 nm underwent a gradual drop with prolonging electrolysis up to attain final increasing removals of 76%, 79% and 85% for raising j values of 7.1, 17.8 and 70 mA cm^{-2}. This trend is indicative of the generation of more absolute quantities of $MO_x(OH)$ and MO_{x+1} radicals at the RuO_2 surface with increasing j, as expected from the concomitant acceleration of the respective reactions (1) and (2). However, a growth of 10-fold of j from 7.1 to 70 mA cm^{-2} only caused an enhancement of 9% in color removal, suggesting a progressive relative loss of oxidants when E_{cell} varied from 4.5 to 8.1 V. This can be related to a greater increase in rate of reaction (2) compared to that of reaction (1) with production of a larger proportion of MO_{x+1} radicals with much lower oxidation ability than $MO_x(OH)$ ones. Moreover, the enhancement of other parasitic reactions can influence the relative decrease of these oxidants,

pre-eminently their oxidation to O_2 via reactions (6) and (7) [8,10], although the formation of weak oxidants like peroxodisulfate ($S_2O_8^{2-}$) ion from SO_4^{2-} oxidation by reaction (8) as previously reported in several works [48-50] and ozone by reaction (9) [5,8] could also contribute.

$$MO_x(OH) \rightarrow MO_x + 1/2O_2 + H^+ + e^- \quad (6)$$

$$MO_{x+1} \rightarrow MO_x + 1/2O_2 \quad (7)$$

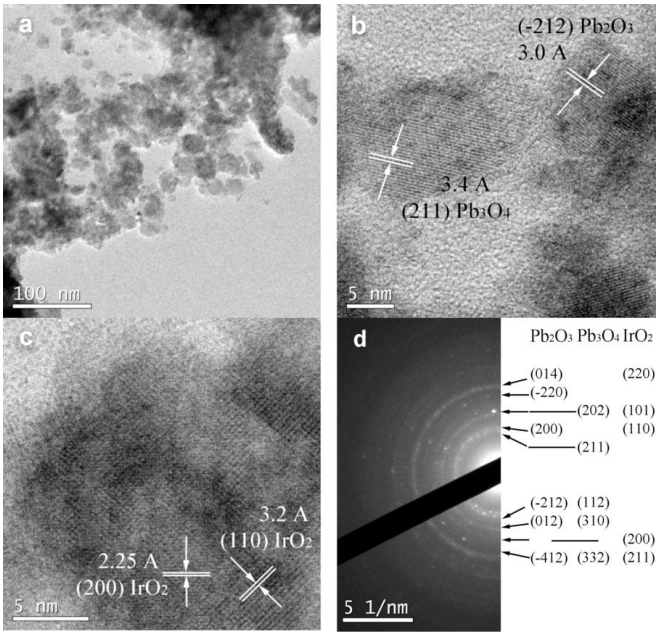

Fig. 3. (a) TEM images corresponding to Ti/Ir-Pb film. (b) HRTEM images for Pb_2O_3 and Pb_3O_4 particles and planes, (c) HRTEM images for IrO_2 particles and plane and (d) SAED patterns with the plans assigned to the Pb_2O_3, Pb_3O_4 and IrO_2 structures.

$$SO_4^{2-} \rightarrow S_2O_8^{2-} + 2\ e^- \quad (8)$$

$$3\ H_2O \rightarrow O_3 + 6\ H^+ + 6\ e^- \quad (9)$$

The effect of the content of the electrolyte background was assessed for a 50 mg dm^{-3} azo dye solution using the same electrodes. Fig. 4b shows the evolution of color removal for 0.050 and 0.50 mol dm^{-3} Na_2SO_4 at j = 70 mA cm^{-2}. Surprisingly, the increase in Na_2SO_4 concentration gave rise to a final slight drop in color abatement from 81% to 73% when changing from 0.050 to 0.50 mol dm^{-3}, along with the decay of E_{cell} from 8.1 to 5.5 V due to the corresponding rise of conductivity, making the process less expensive. This behavior can be associated to the generation of less oxidants at higher Na_2SO_4 content as a result of the deceleration of reactions (1) and (2) due to the lower E_{cell} applied and a higher production of $S_2O_8^{2-}$ from reaction (8), thus limiting the extent of the two above reactions. Comparison of data of Fig. 4a and 4b at j = 70 mA cm^{-2} allows inferring a slight decay of decolorization efficiency when the dye content grew from 30 to 50 mg dm^{-3}, achieving final color removals of 85% and 81%, respectively. This trend is expected for the presence of more organic load that has to be destroyed by similar amounts of oxidants generated at the same j value. Nevertheless, the small difference between both percentage of color removal-time plots suggests a quicker degradation process at higher dye content because of the faster destruction of more organics with greater quantities of oxidants proceeding from the deceleration of parasitic reactions like reactions (6)

and (7).

Several AO assays with the Ti/RuO_2 anode were also performed with a Ti cathode. Fig. 4c evidences that a 50 mg dm^{-3} methyl orange solution in 0.050 mmol dm^{-3} Na_2SO_4 was decolorized up to 81% using a 316 stainless steel cathode, slightly diminishing to 77% using a Ti one. Since the decolorization process of methyl orange is expected to involve its removal along with the slower destruction of its colored byproducts that absorb at the same λ_{max} = 465 nm, as demonstrated for other dyes [5,7,45], the superiority of the 316 stainless steel cathode could be related to the reduction on its surface of a small proportion of byproducts favoring the color decay. This point was confirmed by comparatively studying the decolorization of the above solution with a synthesized Ti/Pt-Pd anode and either a 316 stainless

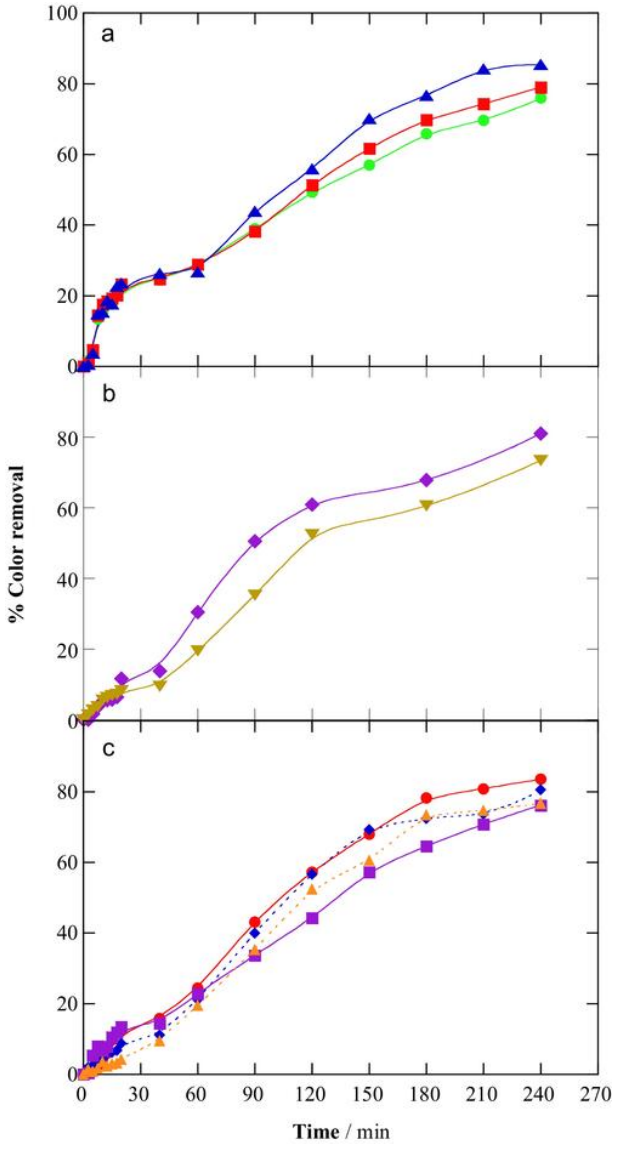

Fig. 4. Effect of operation parameters on the percentage of color removal with electrolysis time for the anodic oxidation (AO) treatment of 2 dm^3 of methyl orange solutions at pH 7.0 and 25 °C. (a) 30 mg dm^{-3} dye in 0.050 mol dm^{-3} Na_2SO_4, Ti/RuO_2 anode and 316 stainless steel cathode, current density (j) of: (green) 7.1 mA cm^{-2}, (red square) 17.8 mA cm^{-2} and (blue triangle) 70 mA cm^{-2}. (b) 50 mg dm^{-3} dye in (blue romboid) 0.050 and (orange) 0.50 mol dm^{-3} Na_2SO_4, with the same electrodes at j = 70 mA cm^{-2}. (c) 50 mg dm^{-3} dye in 0.050 mol dm^{-3} Na_2SO_4, Ti/P**t**-Pd anode and (red circle) 316 stainless steel or (purple) Ti/RuO_2 cathode, Ti/RuO_2 anode and (blue romboid) 316 stainless steel or (orange) Ti cathode, at j = 70 mA cm^{-2}.

steel or a Ti/RuO_2 cathode. Fig. 4c shows a more rapid decolorization using the former cathode to reach 84% color removal, a value higher than 77% obtained for the second one. From these findings, one can conclude that the use of the 316 stainless steel cathode is preferable for the degradation of methyl orange solutions by AO, at least for its decolorization process.

3.3. Comparative degradation of methyl orange solutions using dimensionally stable anodes

Taking into account the above results, the relative oxidation power of the synthesized anodes in AO was assessed for a 50 mg dm^{-3} dye solution of pH 7.0 upon the most favorable conditions of 0.050 mol dm^{-3} Na_2SO_4, a 316 stainless cathode and j = 70 mA cm^{-2}. Under these conditions, similar E_{cell} values of 8.1, 8.1, 8.0, 8.2 and 8.1 V were applied using Ti/Ir-Pb, Ti/Ir-Sn, Ti/Ru-Pb, Ti/Pt-Pd and Ti/RuO_2, respectively. Fig. 5a highlights that at the end of the AO treatment, 96-98% color was removed for Ti/Ir-Pb, Ti/Ir-Sn and Ti/Ru-Pb, whereas only 84% and 81% of color removal were found for Ti/Pt-Pd and Ti/RuO_2, respectively. This indicates that the combination of an active with a non-active material yields an active MMO anode with higher oxidation power that only active materials like Pt, Pd and RuO_2 because of the larger contribution of reaction (1) at the non-active anode surface to generate more quantity of stronger physisorbed $MO_x(OH)$ radicals.

To better understand the behavior of these electrodes in the decolorization of the azo dye solution, the above absorbance decays were analyzed by kinetic equations related to simple reaction orders. The good linear correlations obtained for a pseudo-first-order process are presented in Fig. 5b. From this analysis, decreasing apparent decolorization rate constants (k_{dec}) of 1.76×10^{-2} min^{-1} (R^2 = 0.991) for Ti/Ir-Sn, 1.56×10^{-2} min^{-1} (R^2 = 0.996) for Ti/Ir-Pb, 1.41×10^{-2} min^{-1} (R^2 = 0.990) for Ti/Ru-Pb, 8.0×10^{-3} min^{-1} (R^2 = 0.987) for Ti/Pt-Pd

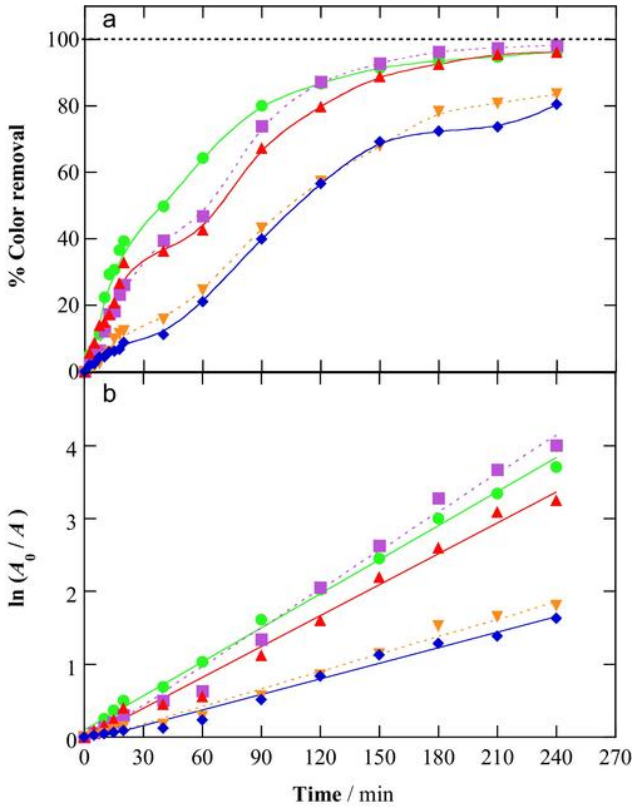

Fig. 5. (a) Percentage of color removal with electrolysis time for the treatment of 2 dm^3 of a 50 mg dm^{-3} methyl orange solution in 0.050 mol dm^{-3} Na_2SO_4 of pH 7 by AO with a 316 stainless steel cathode at j = 70 mA cm^{-2} and 25 °C. Anode: (green) Ti/I**r**-Pb, (purple) Ti/I**r**-Sn, (red) Ti/R**u**-Pb, (orange) Ti/P**t**-Pd, and (blue) Ti/RuO_2. (b) Kinetic analysis of the absorbance decay considering a pseudo-first-order process.

and 7.1×10^{-3} min^{-1} (R^2 = 0.991) for Ti/RuO_2 were determined. The greater k_{dec} found for Ti/Ir-Sn compared to Ti/Ir-Pb seems contradictory to the superior percentage of color removal obtained for the latter anode up to 90 min, as shown in Fig. 5a, but after this time the solution was more quickly decolorized by the former anode and this caused its higher k_{dec} value. The pseudo-first-order decolorization process obtained in all cases suggests that methyl orange and its colored byproducts were always destroyed by a constant amount of oxidants produced upon the steady conditions tested.

Fig. 6a shows the TOC-time plots for the treatment of the 50 mg dm^{-3} methyl orange solution by the different dimensionally stable anodes. In all cases TOC was rapidly removed up to 90-120 min of electrolysis, whereupon the mineralization rate was strongly inhibited due to the formation of byproducts that are hardly destroyed by the oxidizing species. The oxidation power of the anodes for mineralization grew in the order: Ti/RuO_2 < Ti/Pt-Pd < Ti/Ru-Pb < Ti/Ir-Sn < Ti/Ir-Pb, achieving 53.1%, 62.5%, 64.8%, 65.3% and 74.0% at 240 min of electrolysis, respectively. The MMO anodes composed of an active and a non-active material showed again a larger ability to mineralize the methyl orange solution. This means that the physisorbed MO_x(OH) radicals produced at the surface of the Sn and Pb oxides attack more effectively the byproducts originated, favoring their faster mineralization. Our results indicate that the active Ir oxide in the MMO leads to higher TOC removal than active Ru one, probably because some by-products are adsorbed onto its surface enhancing their destruction to much larger extent pre-eminently with the non-active Pb oxide.

The mineralization of the above methyl orange solution is expected

to involve the conversion of the heteroatom N (6.42 mg dm^{-3}, 0.458 mmol dm^{-3}) into inorganic ions. This was corroborated by

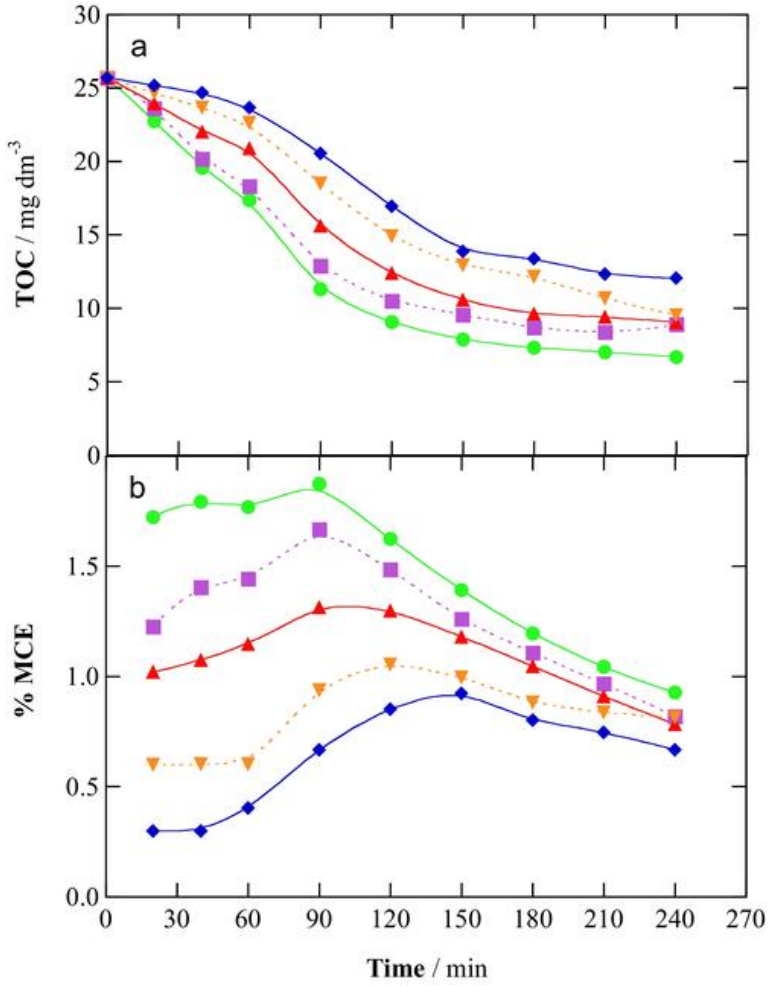

Fig. 6. (a) TOC decay and (b) mineralization current efficiency for the assays of Fig. 5.

quantifying the released nitrogenated ions in the final solution treated with the Ti/Ir-Pb anode. Neither NO_2^- nor NO_3^- were detected, but 2.67 mg dm^{-3} of NH_4^+ (2.3% of initial N) were obtained. This means that NH_4^+ was the preponderant ion released, as proposed in reaction (4). The TN analysis of this solution revealed the presence of 2.04 mg dm^{-3} of N (31.7% of initial N), which can be mainly ascribed to hardly oxidizable *N*-organics remaining in it. This means that 68.3% of initial N was released from the solution during the AO treatment, probably producing volatile N_2 and NO_x species, as established for other *N*-compounds [5,51]. On the other hand, total loss of SO_4^{2-} from the $-SO_3^-$ group was found, as also determined for the electrochemical degradation of dyes with this functional group [5].

Fig. 6b depicts the change in MCE calculated from Eq. (5) for the assays shown in Fig. 6a. The current efficiency always increased at the beginning of the process while the dye was more rapidly mineralized, attaining decreasing maximum contents of 1.88% at 90 min for Ti/Ir-Pb, 1.67% at 90 min for Ti/Ir-Sn, 1.31% at 90 min for Ti/Ru-Pb, 1.05% at 120 min for Ti/Pt-Pd and 0.92% at 150 min for Ti/RuO_2. At longer time, the strong deceleration of the mineralization process caused a gradual and dramatic drop of MCE to reach from 0.93% for the former anode to 0.66% for the latter one. These low current efficiencies

could be strongly improved operating at lower j values, as determined for the AO process of other dyes [5].

3.4. Identification of stable byproducts and proposal of a reaction sequence

The electrochemical oxidation of azo dyes leads to short-chain carboxylic acids as final byproducts [5,7,45]. This behavior was corroborated by analyzing the AO process of the 50 mg dm^{-3} methyl orange solution with a Ti/Ir-Pb anode at j = 70 mA cm^{-2} by means of ion-exclusion HPLC. Malic, succinic and acetic acids coming from the cleavage of the benzene rings of the azo dye [7,13,45,46] were detected, along with the ultimate oxalic and oxamic acids that are directly mineralized to CO_2 [52,53]. Oxalic acid proceeds from the oxidation of longer carboxylic acids, whereas oxamic acid is expected to be produced from the oxidation of *N*-derivatives. Fig. 7 highights that malic, succinic and oxamic acids were accumulated up to 6.50 mg dm^{-3} as maximal, being completely removed at the end of electrolysis. In contrast, high contents of 14.99 and 25.51 mg dm^{-3} of

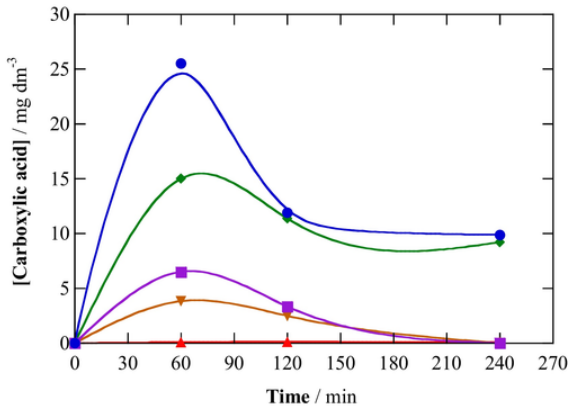

Fig. 7. Time-course of the concentration of: (yellow) malic, (purple) succinic, (green) acetic, (black) oxalic and (red) oxamic acids during the AO degradation of 2 dm^3 of 50 mg dm^{-3} methyl orange in 0.050 mol dm^{-3} Na_2SO_4 at pH 7.0 using a Ti/Ir-Pb anode and a 316 stainless steel cathode at j = 70 mA cm^{-2} and 25 °C.

acetic and oxalic acids, respectively, were accumulated at 60 min, finally decreasing to 9.20 and 9.87 mg dm^{-3}. A mass balance of all carboxylic acids remaining at 240 min revealed that they contribute as 6.32 mg dm^{-3} of TOC, related to a 94.6% of the organic matter contained in the final solution (see Fig. 6a). This means that the AO treatment of methyl orange solutions yielded a mixture of short-linear carboxylic acids, which can explain the inhibition of the mineralization process for times >90 min when they are preferentially and slowly destroyed. This is beneficial for this process since it could be applied during short time for ensuring the conversion of organics into carboxylic acids and the remaining solution could be further treated biologically. This coupled AO-biological treatment will be much more inexpensive and viable in practice.

Two cyclic compounds (hydroquinone and *p*-benzoquinone), 2,3-dimethylbutanol, *N*,*N*-dimethylformamide and another carboxylic acid (isobutiric acid) were also identified from GC-MS analysis of the above treated azo dye solution. From these byproducts and the carboxylic acids detected by ion-exclusion HPLC, the reaction sequence of Fig. 8 is proposed for the mineralization of methyl orange by AO with Ti/Ir-Pb anode. The main oxidizing agent is $MO_x(OH)$ formed from reaction (1) at the surface of Ir oxide and pre-eminently at that of Pb oxide, although slower reactions with MO_{x+1} species and

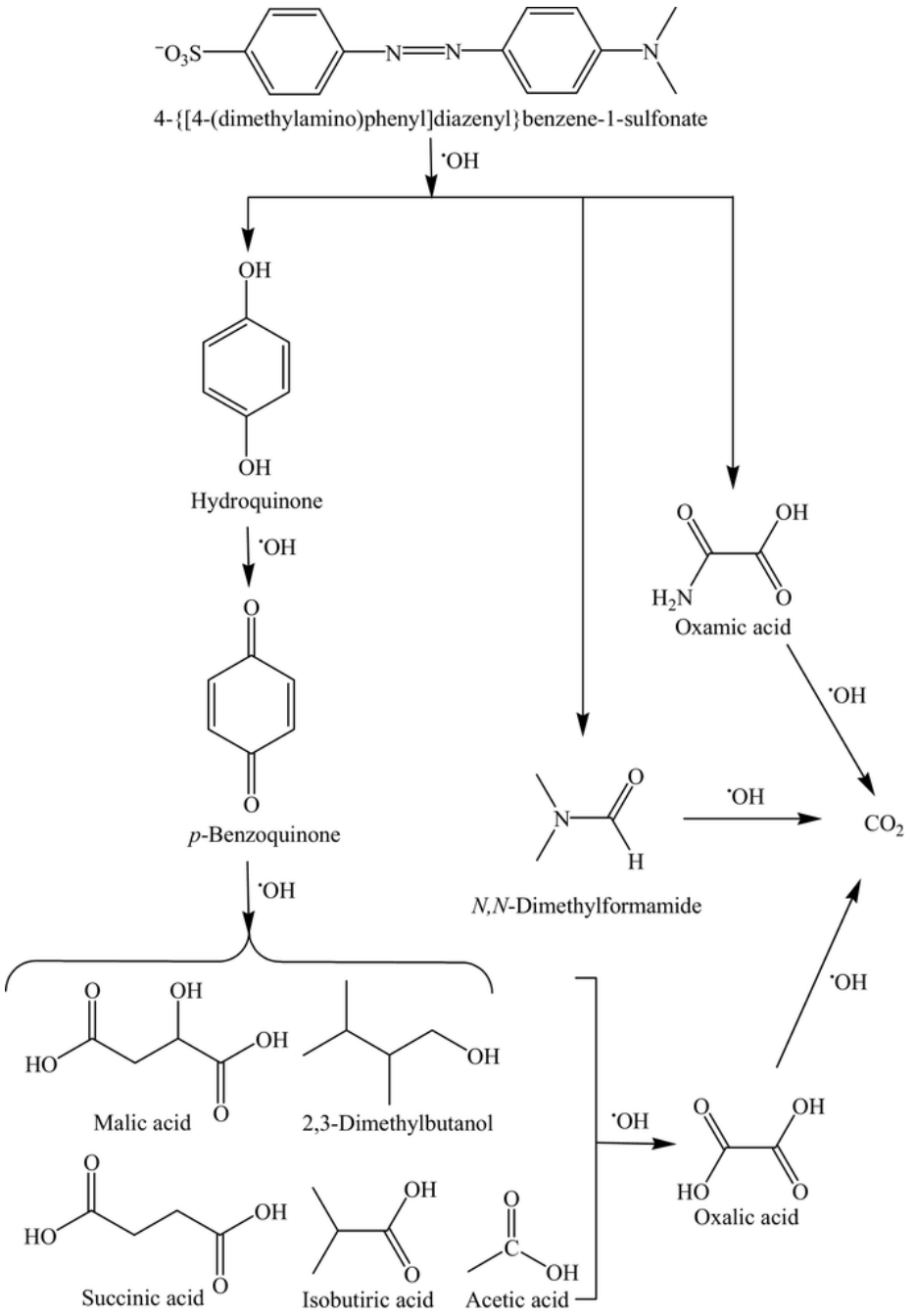

Fig. 8. Proposed reaction sequence for methyl orange mineralization by AO using a Ti/I**r**-Pb anode. OH denotes the main oxidant physisorbed hydroxyl radical originated at the anode surface from water oxidation.

other oxidants like $S_2O_8^{2-}$ ion and O_3 are feasible as well. The process is initiated by the cleavage of the N N bond with formation of small molecules. Hydroxylation of the benzenic rings with the loss of $-SO_3^-$ and amino groups leads to hydroquinone, which is subsequently oxidized to *p*-benzoquinone. Two *N*-derivatives, *N*,*N*-dimethylformamide and oxamic acid, are independently produced as well, being mineralized to CO_2. Degradation of *p*-benzoquinone yields 2,3-dimethylbutanol and a mixture of carboxylic acids includingmalic, succinic, isobutiric and acetic acids. Independent oxidation of these compounds gives finally oxalic acid that is directly transformed into CO_2.

4. Conclusions

Good dimensionally stable anodes of Ti/Ir-Pb, Ti/Ir-Sn, Ti/Ru-Pb, Ti/Pt-Pd and Ti/RuO_2 have been synthesized by the dipping method using metallic chlorides in isopropanol/water. The Ti/Ir-Pb electrode has been characterized by FE-SEM, roughness, EDX, XRD and TEM. It was found that the most powerful Ti/Ir-Pb anode contained a mixture of IrO_2, Pb_2O_3 and Pb_3O_4. The decolorization of methyl orange solutions of pH 7.0 by AO with Ti/RuO_2 was enhanced at j = 70 mA cm^{-2}, using 0.050 instead of 0.50 mol dm^{-3} Na_2SO_4 concentration and a 316 stainless steel cathode. Operating under these favorable conditions, almost total decolorization was attained for Ti/Ir-Pb, Ti/Ir-Sn and Ti/Ru-Pb anodes in 240 min, with lower color removal for Ti/Pt-Pd and Ti/RuO_2 ones. A pseudo-first-order process for color removal at λ_{max} = 465 nm was always found. The oxidation power of the anodes for azo dye mineralization increased in the sequence Ti/RuO_2 < Ti/Pt-Pd < Ti/Ru-Pb < Ti/Ir-Sn < Ti/Ir-Pb, although only 76.0% TOC decay was obtained for the latter electrode. The mixture of active and non-active materials in MMO electrodes favored their oxidation ability compared to only active ones. This was related to the enhancement of the oxidation action of $MO_x(OH)$ in the non-active oxide over that of MO_{x+1}, preponderant in the active oxide. Better results were found using IrO_2 than RuO_2, suggesting the existence of greater adsorption of organics on its surface that favors the attack of oxidizing agents on them. Five stable byproducts were identified by GC-MS and other five short-linear aliphatic carboxylic acids were detected by ion-exclusion HPLC during the AO of the azo dye with Ti/Ir-Pb anode. The formation of such carboxylic acids to large extent at short electrolysis time suggests the use of a coupled AO-biological treatment to design a much more inexpensive and viable process for the azo dye mineralization. A reaction sequence for this process is proposed taking into account all intermediates detected.

Acknowledgements

The authors received financial support from L'Oreal-Unesco through the 9th Edition of Spanish 'For Women in Science' and 2015 edition of 'International Rising Talents' programmes (awarded to Dr. Pellicer), and ENV-BIO-PORAL through the project MAT2014-57960-C3-1-R, and the 2014-SGR-1015 project from the Generalitat de Catalunya. The authors are also indebted to CONACYT (Consejo Nacional de Ciencia y Tecnologia, Mexico) for the grant given to E. Isarain-Chavez.

Appendix A. Supplementary data

Supplementary data associated with this article can be found, in the online version, at http://dx.doi.org/10.1016/j.electacta.2017.05.101.

References

[1] C. Flox, P.L. Cabot, F. Centellas, J.A. Garrido, R.M. Rodriguez, C. Arias, E. Brillas, Electrochemical combustion of herbicide mecoprop in aqueous medium using a flow reactor with a boron-doped diamond anode, Chemosphere 64 (2006) 892-902.
[2] M.T. Fukunaga, J.R. Guimaraes, R. Bertazzoli, Kinetics of the oxidation of formaldehyde in a flow electrochemical reactor with TiO_2/RuO_2 anode, Chem. Eng. J. 136 (2008) 236-241.
[3] M. Zhou, H. Sarkka, M. Sillanpaa, A comparative experimental study on methyl orange degradation by electrochemical oxidation on BDD and MMO electrodes, Sep. Purif. Technol. 78 (2011) 290-297.
[4] A.N.S. Rao, V.T. Venkatarangaiah, Metal oxide-coated anodes in wastewater

treatment, Environ. Sci. Pollut. Res. 21 (2014) 3197-3217.
[5] E. Brillas, C.A. Martinez-Huitle, Decontamination of wastewaters containing synthetic organic dyes by electrochemical methods. An updated review, Appl. Catal. B: Environ. 166-167 (2015) 603-643.
[6] M.J. Santos, M.C. Medeiros, T.M.B.F. Oliveira, C.C. Morais, S.E. Mazzetto, C.A. Martinez-Huitle, S.S. Castro, Electrooxidation of cardanol on mixed metal oxide (RuO_2-TiO_2 and IrO_2-RuO_2-TiO_2) coated titanium anodes: insights into recalcitrant phenolic compounds, Electrochim. Acta 212 (2016) 95-101.
[7] F.C. Moreira, R.A.R. Boaventura, E. Brillas, V.J.P. Vilar, Electrochemical advanced oxidation processes: A review on their application to synthetic and real wastewaters, Appl. Catal. B: Environ 202 (2017) 217-261.
[8] M. Panizza, G. Cerisola, Direct and mediated anodic oxidation of organic pollutants, Chem. Rev. 109 (2009) 6541-6569.
[9] M. Panizza, G. Cerisola, Electrochemical degradation of methyl red using BDD and PbO_2 anodes, Ind. Eng. Chem. Res. 47 (2008) 6816-6820.
[10] C. Comninellis, Electrocatalysis in the electrochemical conversion/combustion of organic pollutants for waste water treatment, Electrochim. Acta 39 (1994) 1857-1862.
[11] B. Boye, P.A. Michaud, B. Marselli, M.M. Dieng, E. Brillas, C. Comninellis, Anodic oxidation of 4-chlorophenoxyacetic acid on synthetic boron-doped diamond electrodes, New Diam. Front. Carbon Technol. 12 (2002) 63-72.
[12] B. Marselli, J. Garcia-Gomez, P.A. Michaud, M.A. Rodrigo, C. Comninellis, Electrogeneration of hydroxyl radicals on boron-doped diamond electrodes, J. Electrochem. Soc. 150 (2003) D79-D83.
[13] E. Isarain-Chavez, R.M. Rodriguez, P.L. Cabot, F. Centellas, C. Arias, J.A. Garrido, E. Brillas, Degradation of pharmaceutical beta-blockers by electrochemical advanced oxidation processes using a flow plant with a solar compound parabolic collector, Water Res. 45 (2011) 4119-4130.
[14] E. Bezerra Cavalcanti, S. Garcia-Segura, F. Centellas, E. Brillas, Electrochemical incineration of omeprazole in neutral aqueous medium using a platinum or boron-doped diamond. Degradation kinetics and oxidation products, Water Res 47 (2013) 1803-1815.
[15] D. Rajkumar, J.G. Kim, Oxidation of various reactive dyes with in situ electro-generated active chlorine for textile dyeing industry wastewater treatment, J. Hazard. Mater. 136 (2006) 203-212.
[16] E. Forgacs, T. Cserhati, G. Oros, Removal of synthetic dyes from wastewaters: a review, Environ. Int. 30 (2004) 953-971.
[17] H. Zollinger, Color Chemistry: Synthesis, Properties, and Applications of Organic Dyes and Pigments, VHCA and Wiley-VCH, Switzerland, 2003.
[18] A.B. dos Santos, F.J. Cervantes, J.B. van Lier, Review paper on current technologies for decolourisation of textile wastewaters: perspectives for anaerobic biotechnology, Bioresour. Technol. 98 (2007) 2369-2385.
[19] S.M.A.G. Ulson de Souza, E. Forgiarini, A.A. Ulson de Souza, Toxicity of textile dyes and their degradation by the enzyme horseradish peroxidase (HRP), J. Hazard. Mater 147 (2007) 1073-1078.
[20] K.P. Sharma, S. Sharma, S.P. Sharma, K. Singh, S. Kumar, R. Grover, P.K. Sharma, A comparative study on characterization of textile wastewaters (untreated and treated) toxicity by chemical and biological tests, Chemosphere 69 (2007) 48-54.
[21] V.J.P. Vilar, L.X. Pinho, A.M.A. Pintor, R.A.R. Boaventura, Treatment of textile wastewaters by solar-driven advanced oxidation processes, Solar Energy 85 (2011) 1927-1934.
[22] V. Khandegar, A.K. Saroha, Electrocoagulation for the treatment of textile industry effluent-a review, J. Environ. Manage. 128 (2013) 949-963.
[23] F. Zaviska, P. Drogui, J.F. Blais, G. Mercier, In situ active chlorine generation for the treatment of dye-containing effluents, J. Appl. Electrochem. 39 (2009) 2397-2408.
[24] K.S. Wang, M.C. Wei, T.H. Peng, H.C. Li, S.J. Chao, T.F. Hsu, S.H. Chang, Treatment and toxicity evaluation of methylene blue using electrochemical oxidation, fly ash adsorption and combined electrochemical oxidation-fly ash adsorption, J. Environ. Manage. 91 (2010) 1778-1784.
[25] S. Singh, S.L. Lo, V.C. Srivastav, A.D. Hiwarkar, Comparative study of electrochemical oxidation for dye degradation: parametric optimization and mechanism identification, J. Environ. Chem. Eng. 4 (2016) 2911-2921.
[26] D.A. Carvalho, J.H. Bezerra-Rocha, N.S. Fernandes, D.R. Da Silva, C.A. Martinez-Huitle, Application of electrochemical oxidation as alternative for removing methyl green dye from aqueous solutions, Latin Am. Appl. Res. 41 (2011) 127-133.
[27] E. Kusmierek, E. Chrzescijanska, M. Szadkowska-Nicze, J. Kaluzna-Czaplinska, Electrochemical discolouration and degradation of reactive dichlorotriazine dyes: reaction pathways, J. Appl. Electrochem 41 (2011) 51-62.
[28] T. Panakoulias, P. Kalatzis, D. Kalderis, A. Katsaounis, Electrochemical degradation of Reactive Red 120 using DSA and BDD anodes, J. Appl. Electrochem. 40 (2010) 1759-1765.
[29] A.I. Del Rio, J. Molina, J. Bonastre, F. Cases, Study of the electrochemical oxidation and reduction of C.I. Reactive Orange 4 in sodium sulphate alkaline solutions, J. Hazard. Mater. 172 (2009) 187-195.

[30] S.H. Li, Y. Zhao, J. Chu, W.W. Li, H.Q. Yu, G. Liu, Electrochemical degradation of methyl orange on Pt-Bi/C nanostructured electrode by a square-wave potential method, Electrochim. Acta 92 (2013) 93-101.
[31] K.T. Chung, G.E. Fulk, A.W. Andrews, Mutagenic testing of some commonly used dyes, Appl. Environ. Microbiol. 42 (1981) 641-648.
[32] M.H. Do, N.H. Phan, T.D. Nguyen, T.T.S. Pham, V.K. Nguyen, T.T.T. Vu, T.K.P. Nguyen, Activated carbon/Fe_3O_4 nanoparticle composite: Fabrication, methyl orange removal and regeneration by hydrogen peroxide, Chemosphere 85 (2011) 1269-1276.
[33] H. Zhang, L. Duan, D. Zhang, Decolorization of methyl orange by ozonation in combination with ultrasonic irradiation, J. Hazard. Mater. 138 (2006) 53-59.
[34] W. Nam, J. Kim, G. Han, Photocatalytic oxidation of methyl orange in a three-phase fluidized bed reactor, Chemosphere 47 (2002) 1019-1024.
[35] N. Guettai, H.A. Amar, Photocatalytic oxidation of methyl orange in presence of titanium dioxide in aqueous suspension. Part I: parametric study, Desalination 185 (2005) 427-437.
[36] N. Guettai, H.A. Amar, Photocatalytic oxidation of methyl orange in presence of titanium 37,43dioxide in aqueous suspension. Part II: kinetics study, Desalination 185 (2005) 439-448.
[37] Y. He, F. Grieser, M. Ashokkumar, The mechanism of sonophotocatalytic degradation of methyl orange and its products in aqueous solutions, Ultrason. Sonochem 18 (2011) 974-980.
[38] S. Haji, B. Benstaali, N. Al-Bastaki, Degradation of methyl orange by UV/H_2O_2 advanced oxidation process, Chem. Eng. J. 168 (2011) 134-139.
[39] A. Srikhaow, S.M. Smith, Preparation of $Cu_2(OH)_3NO_3$/ZnO, a novel catalyst for methyl orange oxidation under ambient conditions, Appl. Catal. B: Environ. 130 (2013) 84-92.
[40] W. Luo, M.E. Abbas, L. Zhu, K. Deng, H. Tang, Rapid quantitative determination of hydrogen peroxide by oxidation decolorization of methyl orange using a Fenton reaction system, Anal. Chim. Acta 629 (2008) 1-5.
[41] C. Ramirez, A. Saldana, B. Hernandez, R. Acero, R. Guerra, S. Garcia-Segura, E. Brillas, J.M. Peralta-Hernandez, Electrochemical oxidation of methyl orange azo dye at pilot flow plant using BDD technology, J. Ind. Eng. Chem. 19 (2013) 571-579.
[42] Z. Liu, F. Wang, Y. Li, T. Xu, S. Zhu, Continuous electrochemical oxidation of methyl orange waste water using a three-dimensional electrode reactor, J. Environ. Sci. 23 (2011) S70-S73.
[43] Y. Kong, Z.L. Wang, Y. Wang, J. Yuan, Z.D. Chen, Degradation of methyl orange in artificial wastewater through electrochemical oxidation using exfoliated graphite electrode, New Carbon Mater 26 (2011) 459-464.
[44] U. Morales-Ortiz, A. Avila-Garcia, Ruthenium oxide films for selective coatings, Sol. Energy Mater. Sol. Cells 90 (2006) 832-840.
[45] F.C. Moreira, S. Garcia-Segura, V.J.P. Vilar, R.A.R. Boaventura, E. Brillas, Decolorization and mineralization of Sunset Yellow FCF azo dye by anodic oxidation electro-Fenton, UVA photoelectro-Fenton and solar photoelectro-Fenton processes, Appl. Catal. B: Environ. 142-143 (2013) 877-890.
[46] E. Isarain-Chavez, R.M. Rodriguez, J.A. Garrido, C. Arias, F. Centellas, P.L. Cabot, E. Brillas, Degradation of the beta-blocker propranolol by electrochemical advanced oxidation processes based on Fenton's reaction chemistry using a boron-doped diamond anode, Electrochim. Acta 56 (2010) 215-221.
[47] E.S. Gadelmawla, M.M. Koura, T.M.A. Maksoud, I.M. Elewa, H.H. Soliman, Roughness parameters, J. Mater. Process. Technol 123 (2002) 133-145.
[48] L. Vazquez-Gomez, S. Ferro, A. De Battisti, Preparation and characterization of RuO_2-IrO_2-SnO_2 ternary mixtures for advanced electrochemical technology, Appl. Catal. B Environ 67 (2006) 34-40.
[49] C.A. Martinez-Huitle, M.A. Rodrigo, I. Sires, O. Scialdone, Single and coupled electrochemical processes and reactors for the abatement of organic water pollutants: A critical review, Chem. Rev. 115 (2015) 13362-13407.
[50] I. Sires, E. Brillas, M.A. Oturan, M.A. Rodrigo, M. Panizza, Electrochemical advanced oxidation processes: today and tomorrow. A review, Environ. Sci. Pollut. Res. 21 (2014) 8336-8367.
[51] S. Garcia-Segura, E. Mostafa, H. Baltruschat, Could NO_x be released during mineralization of pollutants containing nitrogen by hydroxyl radical? Ascertaining the release of N-volatile species, Appl. Catal. B: Environ. 207 (2017) 376-384.
[52] S. Ferro, C.A. Martinez-Huitle, A. De Battisti, Electroxidation of oxalic acid at different electrode materials, J. Appl. Electrochem. 40 (2010) 1779-1787.
[53] S. Garcia-Segura, E. Brillas, Mineralization of the recalcitrant oxalic and oxamic acids by electrochemical advanced oxidation processes using a boron-doped diamond anode, Water Res. 45 (2011) 2975-2984.